PASJ: Publ. Astron. Soc. Japan **62**, 487–499, 2010 April 25

Spectral-Lag Relations in GRB Pulses Detected with HETE-2

Makoto ARIMOTO,[1] Nobuyuki KAWAI,[1] Katsuaki ASANO,[1] Kevin HURLEY,[2] Motoko SUZUKI,[3] Yujin E. NAKAGAWA,[4] Takashi SHIMOKAWABE,[1] Nicolas Vasquez PAZMINO,[1] Rie SATO,[5] Masaru MATSUOKA,[3] Atsumasa YOSHIDA,[6] Toru TAMAGAWA,[4] Yuji SHIRASAKI,[7] Satoshi SUGITA,[6] Ichiro TAKAHASHI,[6] Jean-Luc ATTEIA,[8] Alexandre PELANGEON,[8] Roland VANDERSPEK,[9] Carlo GRAZIANI,[11] Gregory PRIGOZHIN,[9] Joel VILLASENOR,[9] J. Garrett JERNIGAN,[2] Geoffrey B. CREW,[9] Takanori SAKAMOTO,[12] George R. RICKER,[9] Stanford E. WOOSLEY,[16] Nat BUTLER,[2] Alan LEVINE,[9] John P. DOTY,[9,10] Timothy Q. DONAGHY,[11] Donald Q. LAMB,[11] Edward FENIMORE,[15] Mark GALASSI,[15] Michel BOER,[17] Jean-Pascal DEZALAY,[13] Jean-François OLIVE,[13] João BRAGA,[18] Ravi MANCHANDA,[19] and Graziella PIZZICHINI[14]

[1]*Department of Physics, Tokyo Institute of Technology, 2-12-1 Ookayama, Meguro-ku, Tokyo 152-8551*
arimoto@hp.phys.titech.ac.jp
[2]*Space Sciences Laboratory, University of California, Berkeley, CA 94720-7450, USA*
[3]*Japan Aerospace Exploration Agency (JAXA), 2-1-1 Sengen, Tsukuba, Ibaraki 305-8505*
[4]*RIKEN, 2-1 Hirosawa, Wako, Saitama 351-0198*
[5]*Institute of Space and Astronautical Science/JAXA, 3-1-1 Yoshinodai, Chuo-ku, Sagamihara 252-8510*
[6]*Department of Physics and Mathematics, Aoyama Gakuin University, 5-10-1 Fuchinobe, Chuo-ku, Sagamihara 252-8558*
[7]*National Astronomical Observatory of Japan, 2-21-1 Osawa, Mitaka, Tokyo 181-8588*
[8]*Laboratoire Astrophysique de Toulouse-Tarbes (LATT), Université de Toulouse, CNRS, 14 Avenue Edouard Belin, 31400 Toulouse, France*
[9]*Center for Space Research, Massachusetts Institute of Technology, 77 Vassar Street, Cambridge, MA 02139-4307, USA*
[10]*Noqsi Aerospace Ltd., 2822 South Nova Road, Pine, CO 80470, USA*
[11]*Department of Astronomy and Astrophysics, University of Chicago, 5640 South Ellis Avenue, Chicago, IL 60637, USA*
[12]*Goddard Space Flight Center, NASA, Greenbelt, MD 20771, USA*
[13]*Centre d'Etude Spatiale des Rayonnements, 9 Avenue du Colonel Roche, Toulouse, 31028, France*
[14]*Istituto Nazionale di Astrofisica (INAF)/IASF Bologna, Via Gobetti 101, 40129 Bologna, Italy*
[15]*Los Alamos National Laboratory, PO Box 1663, Los Alamos, NM 87545, USA*
[16]*Department of Astronomy and Astrophysics, University of California at Santa Cruz, 477 Clark Kerr Hall, Santa Cruz, CA 95064, USA*
[17]*Observatoire de Haute-Provence (CNRS/OAMP), F-04870 Saint Michel l'Observatoire, France*
[18]*Instituto Nacional de Pesquisas Espaciais, Avenida Dos Astronautas 1758, Saõ José dos Campos 12227-010, Brazil*
[19]*Department of Astronomy and Astrophysics, Tata Institute of Fundamental Research, Homi Bhabha Road, Mumbai, 400-005, India*

(Received 2009 December 27; accepted 2010 February 17)

Abstract

Using a pulse-fit method, we investigated the spectral lags between the traditional gamma-ray band (50–400 keV) and the X-ray band (6–25 keV) for 8 GRBs with known redshifts (GRB 010921, GRB 020124, GRB 020127, GRB 021211, GRB 030528, GRB 040924, GRB 041006, and GRB 050408), detected with the WXM and FREGATE instruments aboard the HETE-2 satellite. We found several relations for individual GRB pulses between the spectral lag and other observables, such as the luminosity, pulse duration, and peak energy, $E_{\rm peak}$. The obtained results are consistent with those for BATSE, indicating that the BATSE correlations are still valid at lower energies (6–25 keV). Furthermore, we found that the photon energy dependence for the spectral lags can be reconciled with the simple curvature effect model. We discuss the implications of these results from various points of view.

Key words: gamma rays: bursts — gamma rays: observations — radiation mechanisms: non-thermal

1. Introduction

Gamma-Ray Bursts (GRBs) are the most energetic explosions in the universe. Past studies have found that GRBs consist of ultrarelativistic outflows with collimated jets at cosmological distances. However, it is not clear how the central engine forms, and how the electrons or protons are accelerated in shocks and how photons are radiated. In addition, GRBs are quite important as a candidate for distance-indicators. Owing to their very intense brightness, GRBs can be a powerful tool for measuring distances in the high-redshift universe.

One of the characteristics of GRB prompt emission is the spectral lag, which is the time delay in the arrival of lower-energy emission relative to higher-energy emission. Previous analyses were conducted with a sample of many BATSE GRBs between typical energy bands of 25–50 keV and 100–300 keV, by using both the cross correlation function (CCF) (e.g., Norris et al. 2000) and the peak-to-peak difference (e.g., Hakkila et al.

2008). A negative correlation between the spectral lag and the luminosity exists for BATSE GRBs above 25 keV energies. Since we can obtain the intrinsic luminosity of GRBs from the lag–luminosity relation once we measure the spectral lag, the distance of the GRB can be derived from the observed flux. However, it is not clear whether the relation is valid in wider energy bands. In addition, from the results of Hakkila et al. (2008), it has been shown that the spectral lag characterizes each *pulse* rather than the entire burst.

From a theoretical point of view (e.g., Qin et al. 2004), the rise-phase timescale may be responsible for the intrinsic pulse width, while the decay-phase timescale may be determined by geometrical effects (e.g., the curvature effect). The curvature effect (Qin 2002; Qin & Lu 2005; Lu et al. 2006) arises from relativistic effects in a sphere expanding with a high bulk Lorentz factor of $\Gamma = 1/(1-\beta^2)^{1/2} \sim 100$. Because of the curvature of the emitting shell, there will be a time delay between the photons emitted simultaneously in the comoving frame from different points on the surface. However, Zhang, Qin, and Zhang (2007) showed that the curvature effect alone is not sufficient to explain energy-dependent pulse properties obtained from a systematic analysis of the lag and the temporal evolution. An alternative model is an off-axis model proposed by Ioka and Nakamura (2001); further, the time-evolution of shock propagation (Daigne & Mochkovitch 1998, 2003; Bošnjak et al. 2009) may also reproduce the spectral lag and the lag–luminosity relation. Thus, it is not clear that either the curvature effect or other effects cause the spectral lag. While the curvature effect should necessarily affect the pulse profile, the time-evolution of shock propagation or the off-axis model strongly depends on unknown model parameters.

In this paper, in order to unveil the properties of the spectral lag for each pulse, we consider the HETE-2 sample with a wider energy range, especially at the low-energy end (> 2 keV) compared to the BATSE sample. In sections 2 and 3 we explain the sample selection and the pulse-fit method. In section 4, we describe the result of the obtained relations between the spectral lag and other observables, and discuss a detailed energy dependence for the spectral lag in section 5. Finally, we briefly comment on future prospects in section 6.

2. HETE-2 Sample and Selection

On board HETE-2, there were two scientific instruments that are relevant to our study: the FREnch GAmma-ray TElescope (FREGATE), which gave the trigger for GRBs and performed spectroscopy over a wide energy range (6–400 keV); and the Wide-field X-ray Monitor (WXM), which was the key instrument for localizing GRBs to $\sim 10'$, and sensitive to the 2–25 keV energy range, lower than the FREGATE one. The instruments produce two types of data. The survey data were recorded with fixed energy bands and time resolution whenever the instruments were on. The time-tagged data were produced with a fixed duration (several minutes) when the instruments were triggered by bursts. From the time-tagged data, we could produce light curves in arbitrary energy bands, while the BATSE detector generally created light curves only in fixed energy bands (although the BATSE detector actually has time-tagged data, many BATSE GRBs are not fully covered due to the limitation of the memory size for the time-tagged data).

Table 1. GRB samples.

GRB	Redshift	Reference
010921	0.45	Djorgovski et al. (2001)
020124	3.20	Hjorth et al. (2003)
020127	1.9*	Berger et al. (2007)
021211	1.01	Vreeswijk et al. (2003)
030528	0.78	Rau, Salvato, and Greiner (2005)
030725	—	Pugliese et al. (2005)
040924	0.86	Wiersema et al. (2004)
041006	0.72	Stanek et al. (2005)
050408	1.24	Berger, Gladders, and Oemler (2005)
060121	—	de Ugarte Postigo et al. (2006)

* This is a possible value estimated from the afterglow investigation and spectral energy distribution.

We performed the spectral-lag analysis using a sample of 8 GRBs detected by HETE-2 with known or estimated redshifts for studying the lag–luminosity relation described in section 4. Our selection criteria for the GRB samples were as follows: 1) $T_{90} > 2$ s, where T_{90} is the observed duration including 90% of the total observed counts; and 2) time-tagged data are available. For the latter, we note that the time-tagged data were lost for some bursts due to downlink problems or invalidation of the instruments (e.g., GRB030328, GRB030329, etc.). For these bursts, since the available energy band was too coarse for the survey data (e.g., 6–40 keV, 6–80 keV, and 32–400 keV for FREGATE), we could not conduct a detailed study of the spectral lag. For the analysis described in section 4, we used the FREGATE instrument only because off-axis photon events were partially coded, and the number of events detected by the WXM instrument was often small, while the FREGATE instrument detected more photons than the WXM one did due to its relatively large effective area ($\sim 150\,\mathrm{cm}^2$); not all of the selected GRBs had enough photons to perform the analysis in the WXM energy band.

In addition, for studying the detailed energy dependence of the spectral lag for individual GRB pulses described in section 5, we added two GRBs without known redshifts having sufficiently non-overlapped pulses to the sample. In this analysis, we used not only the FREGATE instrument, but also the WXM one, because some GRBs had sufficiently good statistics detected by the WXM instrument. Here, since there were not good statistics in the multiple energy bands for GRB 020124 and GRB 041006, we excluded the two GRBs from the sample.

We give a list of 10 GRBs in table 1 and the energy bands in the burst rest frame which were covered by the WXM and FREGATE instruments for the 8 selected GRBs with known redshifts in figure 1.

3. Method

Each GRB pulse was fitted with a four-parameter pulse model (Norris et al. 2005): if $t > t_{\mathrm{start}}$,

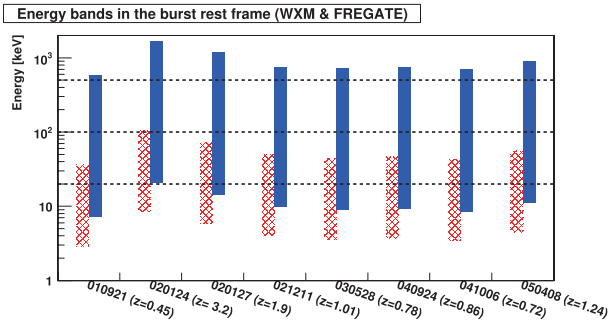

Fig. 1. Energy bands in the burst rest frame for the selected GRBs. The red crosshatched bars represent the WXM bands and the blue solid ones do the FREGATE bands. The adopted energy ranges are between the dashed lines (20–100 keV and 100–500 keV).

$$I(t) = A\lambda \exp[-\tau_1/(t - t_{\rm start}) - (t - t_{\rm start})/\tau_2] + B(t) \quad (1)$$

$$= A\lambda \exp[-\tau_1/(t + \tau_{\rm peak} - t_{\rm peak}) - (t + \tau_{\rm peak} - t_{\rm peak})/\tau_2] + B(t), \quad (2)$$

and if $t < t_{\rm start}$, $I(t) = B(t)$, where I is the intensity, and t is the time after the trigger; τ_1 and τ_2 are the pulse-rise and pulse-decay constants, $\lambda \equiv \exp[2(\tau_1/\tau_2)^{1/2}]$; $t_{\rm peak}$ is the time of the pulse's maximum intensity, A; $t_{\rm start}$ is the start time; $\tau_{\rm peak} \equiv (\tau_1\tau_2)^{1/2}$ is the peak time from the start time, so that $t_{\rm peak} = t_{\rm start} + \tau_{\rm peak}$; $B(t)$ is the background function (we utilize a constant or linear function). In equation (2), $t_{\rm peak}$ is treated as a primary-fitting parameter in order to estimate the uncertainty about $t_{\rm peak}$ directly in the fitting procedure.

The time $t_{\rm start}$ is the formal onset time, and in some cases $t_{\rm start}$ is not indicative of the visually apparent onset time. Especially in the case of $\tau_1 \gg 1$ s, $t_{\rm start}$ is extremely far from the peak of the pulse. Here, as described in Norris et al. (2005), we introduce an effective onset time, $t_{\rm eff}$, arbitrarily defined as the time when the pulse reaches 0.01 times the peak intensity. Furthermore, the values of $t_{\rm eff}$ are different in each energy band. For HETE-2 GRBs, the statistics of GRBs are not as reliable as those of BATSE because, e.g., the effective area of the FREGATE detector ($\sim 150\,{\rm cm}^2$) is smaller than that of the BATSE ($\sim 2000\,{\rm cm}^2$) by a factor of ~ 10. This causes $t_{\rm eff}$ to be scattered in different energy bands due to uncertainties in the determinations of τ_1 and τ_2. To avoid using $t_{\rm eff}$, we adopted an onset time of the "bolometric" light-curve profile, $t'_{\rm eff}$, derived by fitting the light curve in the 6–400 keV band, which corresponds to the entire FREGATE-energy band. The adoption of $t'_{\rm eff}$ is supported by Hakkila and Nemiroff (2009). They showed that the onset of GRB pulses occurs simultaneously across all energy bands. Thus, we define $T_{\rm peak} = t_{\rm peak} - t'_{\rm eff}$ in this paper. The corresponding uncertainties were calculated by using the error propagation formula.

A spectral peak lag is defined as the difference in maximum-intensity time between two energy bands as

$$\tau_{\rm lag} \equiv t_{\rm peak,low} - t_{\rm peak,high}, \quad (3)$$

where "low" and "high" represent the low- and high-energy bands, respectively. Another measurable pulse property is the pulse duration, $w \equiv 3\tau_2[1 + (4/3)(\tau_1/\tau_2)^{1/2}]^{1/2}$, defined as the time intervals where the intensities are equal to $e^{-3}I(t_{\rm peak})$.

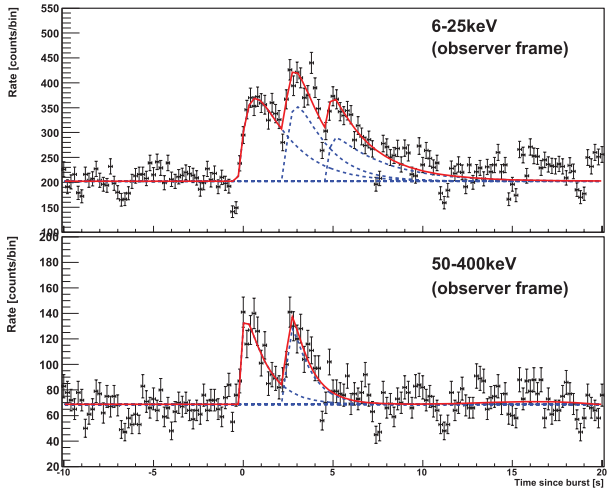

Fig. 2. Pulse fit for GRB 050408 in the 6–25 keV and 50–400 keV bands in the observer's frame.

4. Relation between the Spectral Lag and Other Parameters

In the present work, we adopted two sets of energy bands in order to calculate a spectral lag between two divided bands. The first set was 6–25 keV and 50–400 keV in the observer's frame. Although in a previous study by BATSE the energy-band set of 25–50 keV and 100–300 keV had been adopted, we adopted the lower-energy band (< 25 keV), and tested if the same relation (e.g., lag–luminosity relation) was established or not. Furthermore, for all of the previous studies of the spectral lag, the energy bands refer to the *observer's* frame. However if the spectral lag is a characteristic property of GRBs, it is better to derive the spectral lag between the energy bands in the *burst rest* frame. The HETE-2 time-tagged data have the advantage in such an analysis, compared with the BATSE detector. Thus, we adopted the energy bands of 20–100 keV and 100–500 keV in the burst rest frame covered by the FREGATE instrument. The adopted energy bands are shown as horizontal lines in figure 1.

Here, we used pulses that satisfy the following requirements: the significance of the spectral lag $\sigma_{\rm sig} > 1.5$ and positive lag $\tau_{\rm lag} > 0$, where

$$\sigma_{\rm sig} \equiv \tau_{\rm lag}/\sigma_{\rm lag}, \quad (4)$$

$$\sigma_{\rm lag} \equiv \left(\sigma^2_{\rm peak,low} + \sigma^2_{\rm peak,high}\right)^{1/2}. \quad (5)$$

The value $\sigma_{\rm lag}$ represents the $1\,\sigma$ uncertainty of $\tau_{\rm lag}$, and $\sigma_{\rm peak}$ is defined as the $1\,\sigma$ uncertainty of $t_{\rm peak}$. For a negative lag, its significance is low ($\sigma_{\rm lag} < 1$), and because the number of pulses having a negative lag was very small, we did not take them into account. One of the pulse-fitted results is shown in figure 2 (GRB 050408) by using the χ^2 fitting routine. For the fitting, we fit pulses to make the obtained values of χ^2/d.o.f. (degree of freedom) reasonable (~ 1).

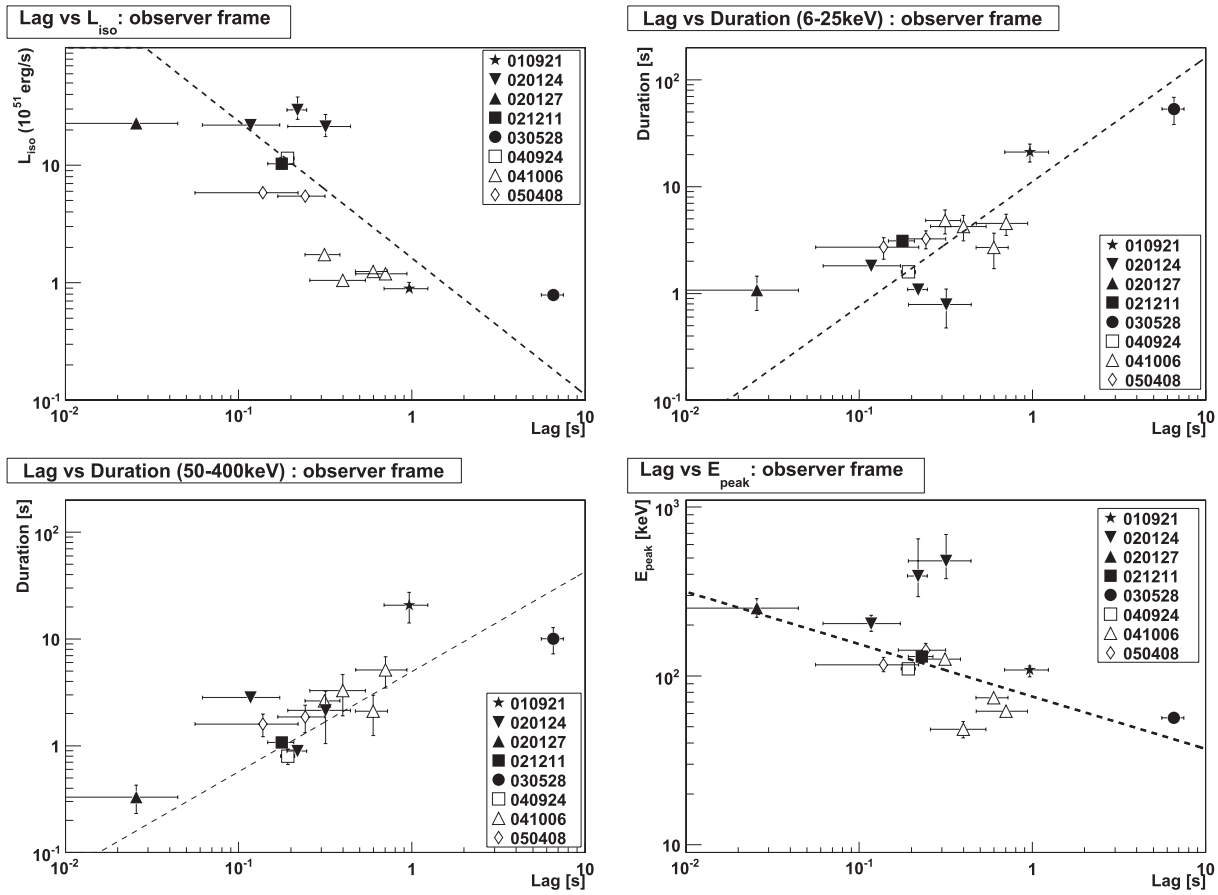

Fig. 3. Scatter plot (observer's frame) of spectral lag vs. luminosity (top left), duration for the low-energy band (top right), duration for the high-energy band (bottom left), and $E_{\rm peak}$ (bottom right). The dashed lines represent the best-fit functions.

4.1. Observer's Frame

First, we show scatter plots of the spectral lag, $\tau_{\rm lag}$, and the luminosity, $L_{\rm iso}$, in the top-left panel of figure 3, where the spectral lag was calculated in the observer's frame. The luminosity in this paper is defined as the average luminosity over the pulse FWHM timescale. As shown in this figure, we can see a negative correlation between the spectral lag and the luminosity. Here, for the correlation coefficient, we adopted the *Spearman rank-order* correlation test. Furthermore, to estimate the correlation coefficient on the basis of the spectral lag's confidence level, we performed a Monte Carlo simulation. Since we had already obtained $\tau_{\rm lag}$, $\sigma_{\rm lag}$, the luminosity, and its uncertainty, we could generate a *pseudo* plot based on the specific probability distributions; that is, we could make a similar plot to the top-left panel of figure 3 with random number seeds. We then calculated the value of the correlation coefficient, R, for the generated *pseudo* plot using the *Spearman rank-order* correlation test. Finally, we repeated the same procedure 10000 times with different random-number seeds. Since we obtained a histogram of the correlation coefficient, we regard the $1\,\sigma$ width as the $1\,\sigma$ confidence level. We adopted this method in the following analysis.

For the lag–luminosity relation in the observer's frame, we obtained the correlation coefficients as $R = -0.79^{+0.16}_{-0.05}$ with a chance probability of 7.7×10^{-4} at the most probable value. The best-fit functional form is $\log(L_{51}) = A_1 + B_1 \log(\tau_{\rm lag})$ with $A_1 = -0.79 \pm 0.04$, $B_1 = -1.16 \pm 0.07$; the reduced chi-square is $133.2/12$ in the observer's frame. Although there are large scatters in the data from the best-fit line, the lag–luminosity relation holds even for the low-energy band (< 25 keV). While our results reconfirm the lag–luminosity relation previously reported, our spectral-lag index (-1.2) is slightly smaller than that of Hakkila et al. (2008) (index ~ -0.6). The slight difference seems to come from the following: (1) the different timescales to estimate the luminosity (BATSE used 256 ms, while we adopt the pulse FWHM timescale); (2) the small numbers of GRB samples for both Hakkila et al. (2008) and HETE-2; (3) the difference in the adopted energy band and/or the instrumental response between Hakkila et al. (2008) and ours. Thus, the slight difference in the power-law index of the correlations between Hakkila et al. (2008) and our results is not surprising.

We show scatter plots of the spectral lags and the durations at low energy in the top-right panel of figure 3 and at high energy in the bottom left. We could find correlations between the spectral lags and durations in both the 6–25 keV and 50–400 keV bands. The best-fit functional forms of these relations are $\log(w_{\rm low}) = A_2 + B_2 \log(\tau_{\rm lag})$ where $A_2 = 1.05 \pm 0.06$, $B_2 = 1.16 \pm 0.09$, and the reduced

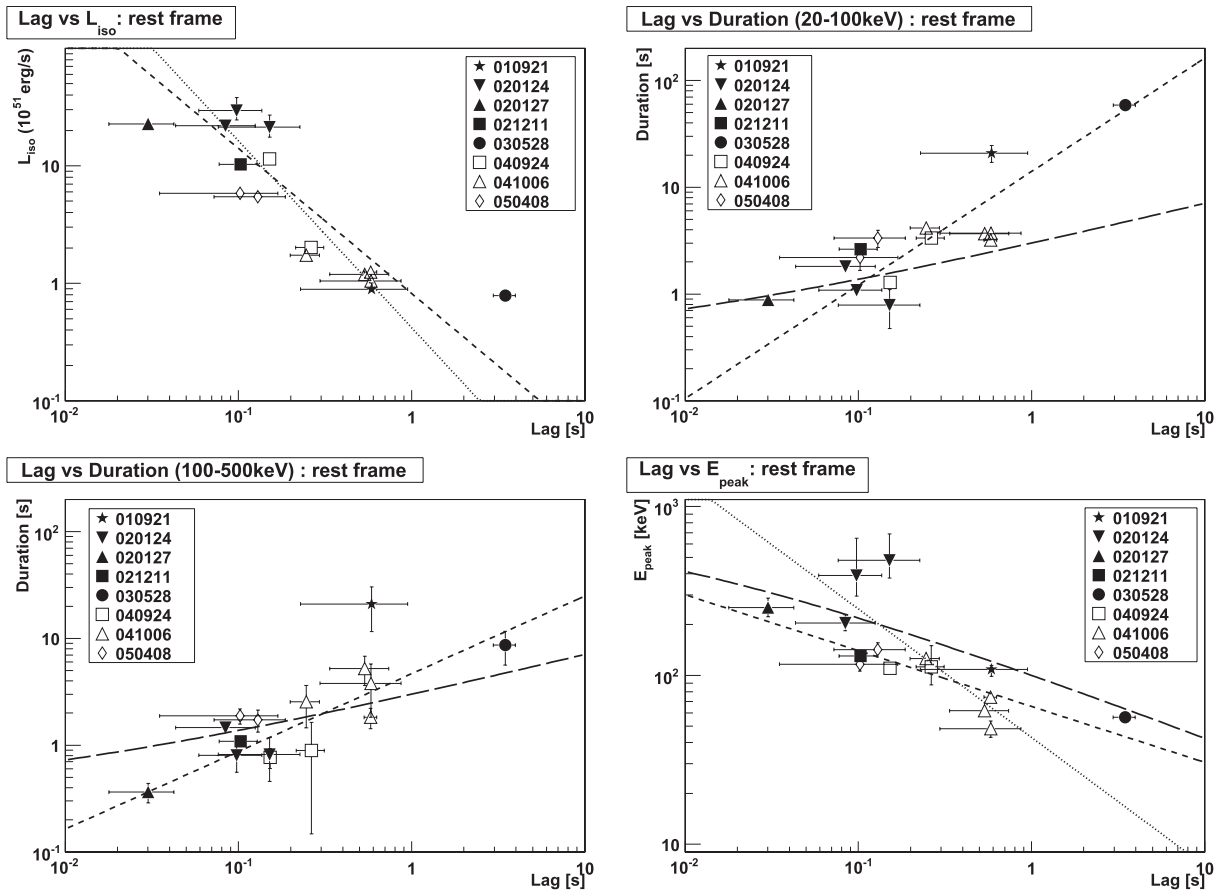

Fig. 4. Scatter plots (burst rest frame) of spectral lag vs. luminosity (top left), duration for the low-energy band (top right), duration for the high-energy band (bottom left), and $E_{\rm peak}$ (bottom right). The dashed lines represent the best-fit functions. For the last three plots, the long dashed lines show the theoretical curves expected in the off-axis model (Ioka & Nakamura 2001). The dotted lines represent the best-fit functions, including the systematic uncertainty and excluding GRB 030528.

chi-square is $43.0/12$ in the 6–25 keV band, and $\log(w_{\rm high}) = A_3 + B_3\log(\tau_{\rm lag})$ with $A_3 = 0.69 \pm 0.05$, $B_3 = 0.94 \pm 0.08$, and $45.1/12$ in the 50–400 keV band. The correlation coefficients are $R = 0.66^{+0.10}_{-0.14}$ and $R = 0.74^{+0.06}_{-0.14}$, and the corresponding chance probabilities at the most probable values in the 6–25 keV and 50–400 keV bands are 1.0×10^{-2} and 2.5×10^{-3}, respectively. The low-chance probabilities assure tight correlations. These results are almost consistent with those of Hakkila et al. (2008) (index 0.85).

Finally, the scatter plot of the spectral lag and peak-time $E_{\rm peak}$ is shown in the bottom-right panel of figure 3 in the observer's frame. The best-fit functional form is $\log(E_{\rm peak}) = A_4 + B_4\log(\tau_{\rm lag})$ with $A_4 = 1.88 \pm 0.02$, $B_4 = -0.31 \pm 0.02$, and the reduced chi-square is $97.8/12$. The correlation coefficient is $R = -0.66^{+0.15}_{-0.08}$ with a chance probability of 1.0×10^{-2}. Thus, we obtained a possible negative correlation between $E_{\rm peak}$ and the spectral lag, though the dependence of the spectral lag on $E_{\rm peak}$ is relatively weak (index ~ -0.3) compared with the other parameters.

4.2. *Burst Rest frame*

We show the results of the relations between the spectral lag and the other parameters in the *burst rest* frame in figure 4 (and the result of the fitted pulses in figure 8), and the adopted energy bands were determined so as to have the same energies in common (20–100 keV and 100–500 keV). With the case for the observer's frame, the best-fit parameters of individual relations are summarized in table 2. We find that there is no significant difference in the result between the observer's frame and the burst rest one. The obtained results support the idea that the cosmological effects should not significantly change our measurement in the observer's frame, even though most GRBs are found at high redshifts. The intrinsic properties for GRB pulses predominate over the cosmological effects, as suggested by Hakkila et al. (2008) and Hakkila and Cumbee (2009).

4.3. *Discussion*

We obtained the correlations between the spectral lag and the other parameters ($L_{\rm iso}$, durations, and $E_{\rm peak}$), in the observer's and the burst rest frames. In particular, our result extends the energy coverage to a lower energy band (6–25 keV). This indicates that the GRB emission in the wide X-ray band has the same origin.

Since there is no significant difference between the result in the observer's frame and that in the burst rest one, it is natural to adopt the burst rest frame to discuss the origin of the spectral lag. Thus, in the following discussion, we refer to the case of the burst rest frame.

Table 2. Fitting parameters determined from the relations of the lag–luminosity, lag–duration, and lag–$E_{\rm peak}$.*

		A	B	Reduced chi-square	Correlation coefficient
Luminosity†	obs	-0.79 ± 0.04	-1.16 ± 0.07	133.2/12	$-0.79^{+0.16}_{-0.05}$
	rest	-1.09 ± 0.04	-1.23 ± 0.07	97.1/13	$-0.90^{+0.12}_{-0.02}$
Duration‡	obs	1.05 ± 0.06	1.16 ± 0.09	43.0/12	$0.66^{+0.10}_{-0.14}$
(low energy)	rest	1.06 ± 0.04	1.15 ± 0.06	72.5/13	$0.74^{+0.06}_{-0.15}$
Duration‡	obs	0.69 ± 0.05	0.94 ± 0.08	45.1/12	$0.74^{+0.06}_{-0.14}$
(high energy)	rest	0.67 ± 0.06	0.73 ± 0.09	26.6/13	$0.72^{+0.07}_{-0.22}$
$E_{\rm peak}$§	obs	1.88 ± 0.02	-0.31 ± 0.02	97.8/12	$-0.66^{+0.15}_{-0.08}$
	rest	1.82 ± 0.02	-0.33 ± 0.03	33.9/13	$-0.81^{+0.16}_{-0.05}$

* Note that "obs" represents the observer's frame and "rest" does the rest frame.
† $\log(L_{51}) = A + B\log(\tau_{\rm lag})$.
‡ $\log(w) = A + B\log(\tau_{\rm lag})$.
§ $\log(E_{\rm peak}) = A + B\log(\tau_{\rm lag})$.

4.3.1. Physical origin of the relations

To account for the relation between the spectral lag and $L_{\rm iso}$, let us consider the off-axis model suggested by Ioka and Nakamura (2001); the detector observes a GRB jet with different viewing angles, θ_v. The intrinsic physical parameters (bulk Lorentz factor, Γ, opening half-angle, $\Delta\theta \sim 1/\Gamma$, shell radius, r_0, from the center, and $E'_{\rm peak}$ in the comoving frame) are assumed to be the same for all GRBs. In the present work, we adopted the same parameters as those of Ioka and Nakamura (2001); $\Gamma\Delta\theta = 1$, $r_0/c\beta\Gamma^2 = 1$. This model assumes an intrinsic spectral shape in the comoving frame, which is approximated by the Band function (Band et al. 1993) as

$$f(E') = \left(\frac{E'}{E_0}\right)^{1+\alpha_{\rm B}} \left[1 + \left(\frac{E'}{E_0}\right)^{s}\right]^{\frac{\beta_{\rm B}-\alpha_{\rm B}}{s}}, \quad (6)$$

where $\alpha_{\rm B}$ and $\beta_{\rm B}$ are the low- and high-energy indices, s describes the smoothness of the transition between the high and low energies, and E_0 is the break energy. Ioka and Nakamura (2001) showed that the observable values, such as the luminosity, the pulse duration (FWHM), w, and the peak energy, $E_{\rm peak}$, change with the viewing angle, $\theta_{\rm v}$, and correlate with the spectral lag as

$$L_{\rm iso} \propto \tau_{\rm lag}^{\frac{-2+\alpha_{\rm B}}{s+1}}, \quad (7)$$

$$w \propto 1 + {\rm const} \times \tau_{\rm lag}^{\frac{1}{s+1}}, \quad (8)$$

$$E_{\rm peak} \propto \left(1 + {\rm const} \times \tau_{\rm lag}^{\frac{1}{s+1}}\right)^{-1}. \quad (9)$$

We obtained $L_{\rm iso} \propto \tau_{\rm lag}^{-1.2}$ from the lag–luminosity relation in figure 4, so that the off-axis model with $s = 1.5$ and the typical value for the low-energy photon index $\alpha_{\rm B} = -1$ can reproduce the lag–luminosity relation.

The expected theoretical results are superimposed on figure 4. Here, we adopt arbitrary normalization values for the theoretical lines. For the lag–duration relation in the high-energy band (100–500 keV), the observational points are consistent with the theoretical curve. For the lag–duration relation in the low-energy band (20–100 keV), the observational points agree with the theoretical curve for small spectral lags, although there are some outliers for large spectral lags. For the lag–$E_{\rm peak}$ relation, we find consistency between the observational points and the theoretical curve. Except for some outliers, we find that the off-axis model can explain the observational results well, even though the model seems to be oversimplified. (All intrinsic physical parameters are common for all GRBs in this model.) Furthermore, for the off-axis model the spectral lag was calculated by using the difference in peak time between the different energy bands, just as we calculated the spectral lag, unlike Norris et al. (2000), in which the spectral lags were calculated by the CCF method.

4.3.2. Yonetoku relation

We now consider the consistency between the observational points and the Yonetoku relation (Yonetoku et al. 2004) in this section. In the preceding section, we found that the off-axis model reproduces the observational results, and did not impose any limitations, such as the Yonetoku relation ($L_{\rm iso} \propto E^2_{\rm peak}$).

Assuming that the Yonetoku relation is valid, from our result on the lag–luminosity relation ($L_{\rm iso} \propto \tau_{\rm lag}^{-1.23\pm0.07}$), the lag–$E_{\rm peak}$ relation is expected to satisfy

$$E_{\rm peak,exp} \propto L_{\rm iso}^{1/2} \propto \tau_{\rm lag}^{-1.23/2} \propto \tau_{\rm lag}^{-0.62}. \quad (10)$$

The index (-0.62) is small compared with the obtained result ($E_{\rm peak,obs} \propto \tau_{\rm lag}^{-0.33\pm0.03}$). Note that the subscripts "exp" and "obs" represent the expected and observed values, respectively.

Let us assume that the determination of the spectral lag has a systematic uncertainty $\sigma_{\rm sys}$ of 0.05 s resulting from the overlaps of the GRB pulses or some calibration uncertainties. In addition, we excluded the peculiar case of GRB 030528, which has a very long spectral lag that may be due to the overlapping of multiple pulses. Then, the best-fit functions became $\log(L_{51}) = (-1.38 \pm 0.13) - (1.59 \pm 0.28)\ \log(\tau_{\rm lag})$ with a reduced chi-square of $\chi^2_\nu = 8.2/12$, and $\log(E_{\rm peak}) = (1.63 \pm 0.08) - (0.76 \pm 0.17)\ \log(\tau_{\rm lag})$ with

a reduced chi-square of $\chi^2_\nu = 12.5/12$. The Yonetoku relation and the revised lag–luminosity relation give

$$E_{\rm peak,exp} \propto \tau_{\rm lag}^{-1.59/2} \propto \tau_{\rm lag}^{-0.80}, \quad (11)$$

which agrees with the revised result (index -0.76). Therefore, considering the small sample and observational uncertainties, we cannot exclude the validity of the Yonetoku relation from our results.

5. Detailed Energy Dependence of Spectral Lag and Other Properties

We next consider the detailed energy dependence of the spectral lag and other properties (the durations including the rise and decay times), besides the lag–luminosity relation described in the previous sections.

5.1. Energy Dependence of Duration, Rise, and Decay Phases

Zhang, Qin, and Zhang (2007) studied the energy dependence of the temporal properties represented by the following formulae:

$$w \propto E^{\alpha_{\rm w}}, \quad (12)$$

$$\tau_{\rm rise} \equiv \frac{1}{2}(w - \tau_2) \propto E^{\alpha_{\rm rise}}, \quad (13)$$

$$\tau_{\rm decay} \equiv \frac{1}{2}(w + \tau_2) \propto E^{\alpha_{\rm decay}}, \quad (14)$$

where $\tau_{\rm rise}$ and $\tau_{\rm decay}$ are the rise and decay timescales (Norris et al. 2005). They found that $\alpha_{\rm w}$ and $\alpha_{\rm decay}$ are highly correlated, while $\alpha_{\rm w}$ and $\alpha_{\rm rise}$ are not strongly correlated. Here, it may be reasonable to assume that the intrinsic pulse width is responsible for the rise-phase timescale, while the decay-phase one is determined by the geometrical effect in the relativistic expanding shell. Furthermore, the decay time interval dominates the duration because the typical pulse shape shows a fast rise and exponential decay (FRED). Thus, it is natural that the decay phase is highly dependent on the duration, and the rise one is not strongly related to the duration (or decay time).

We show the results of plots among $\alpha_{\rm w}$, $\alpha_{\rm rise}$, and $\alpha_{\rm decay}$ in figure 5 (and the result of the fitted pulses in figure 9). The top panel of figure 5 shows a scatter plot of $\alpha_{\rm w}$ versus $\alpha_{\rm rise}$ in our HETE-2 sample. Although the uncertainty for each point is very large, we find a marginal linear relation with a correlation coefficient of $R = 0.51^{+0.18}_{-0.38}$. The best-fit function is $\alpha_{\rm rise} = (0.04 \pm 0.15) + (1.06 \pm 0.41)\alpha_{\rm w}$. If the rise timescale is determined only by the intrinsic pulse width, the correlation between $\alpha_{\rm rise}$ and $\alpha_{\rm w}$ should be weak. However, from this result $\alpha_{\rm w}$ seems to be roughly proportional to $\alpha_{\rm rise}$. Therefore, the rise timescale depends not only on the the intrinsic pulse width, but also somewhat on the geometrical (curvature) effect. Some previous studies may give us clues to an understanding of this behavior; Lu et al. (2007) and Peng et al. (2009) found that $E_{\rm peak}$ decays monotonically through long GRB pulses. This energy decay occurs even prior to the pulse peak, namely in the rise-time phase. Therefore, the pulse-rise phase is a part of the $E_{\rm peak}$-decay phase. Hakkila and Cumbee (2009) also demonstrated that the high-energy pulse intensity starts to decline prior to the pulse peak in the low-energy band, as is the case for the HETE-2 results. Thus, these results indirectly indicate that the pulse-rise timescale is affected by the pulse-decay time.

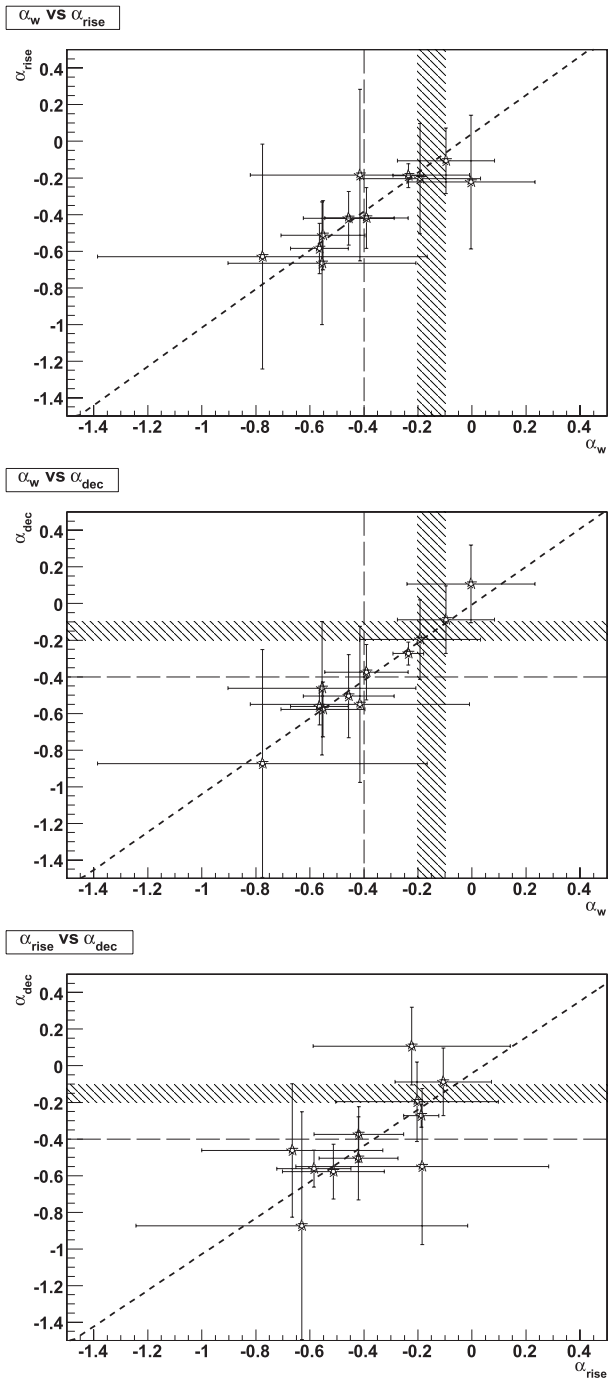

Fig. 5. Scatter plots for indices of $\alpha_{\rm w}$, $\alpha_{\rm rise}$ and $\alpha_{\rm decay}$. (Top): $\alpha_{\rm w}$ vs. $\alpha_{\rm rise}$. (Middle): $\alpha_{\rm w}$ vs. $\alpha_{\rm decay}$. (Bottom): $\alpha_{\rm rise}$ vs. $\alpha_{\rm decay}$. The dashed line shows the best-fit linear function. The shaded area and long vertical- and horizontal-dashed lines represent the expected values from the simple curvature effect (Shen et al. 2005) and the hydrodynamical effect (Daigne & Mochkovitch 1998), respectively.

The middle panel of figure 5 shows a scatter plot of $\alpha_{\rm w}$ versus $\alpha_{\rm decay}$. The best-fit function is $\alpha_{\rm decay} = (-0.01 \pm 0.13) + (1.03 \pm 0.37)\alpha_{\rm w}$ with a correlation coefficient of $R = 0.67^{+0.13}_{-0.37}$. Since a relatively definite correlation between

$\alpha_{\rm w}$ and $\alpha_{\rm decay}$ holds, this result supports the approximation $w \sim \tau_{\rm decay}$ and the assumption that the curvature effect determines the decay timescale.

The relations between $\alpha_{\rm rise}$ versus $\alpha_{\rm decay}$ are plotted in the bottom panel of figure 5, where the best-fit function is $\alpha_{\rm decay} = (-0.04 \pm 0.13) + (0.99 \pm 0.40)\alpha_{\rm rise}$ with a correlation coefficient of $R = 0.46^{+0.20}_{-0.38}$. This result also seems to show that the rise timescale is slightly affected by the curvature effect. Although the uncertainties in the correlation coefficient and the fitting parameter are large, relationships among $\alpha_{\rm w}$, $\alpha_{\rm rise}$, and $\alpha_{\rm decay}$ are consistent with those of Zhang, Qin, and Zhang (2007) (the three functional forms agree with ours).

Shen, Song, and Li (2005) computed the temporal profiles of the GRB pulse in the four BATSE energy bands, with the relativistic curvature effect of an expanding shell. They included an intrinsic "Band"-shape spectrum and an intrinsic energy-independent emission profile, and estimated the dependence of the duration and other properties on the energy as $w \propto E^{-0.2\sim-0.1}$ ($\alpha_{\rm w} \simeq \alpha_{\rm decay} = -0.2$ to -0.1). On the other hand, Daigne and Mochkovitch (1998) calculated the time-evolution of the internal shocks (hydrodynamical effect) assuming a highly nonuniform distribution of the Lorentz factor, and obtained an energy dependence of $w \propto E^{-0.4}$.

In our result, shown in figure 5, $\alpha_{\rm w}$ and $\alpha_{\rm decay}$ range from -0.8 to 0, and the expected energy dependences for the models of Daigne and Mochkovitch (1998) and Shen, Song, and Li (2005) are represented as a long dashed line and a shaded portion, respectively. The data points are widely scattered so that the simple model of Daigne and Mochkovitch (1998) or Shen, Song, and Li (2005) alone cannot explain the results that we obtained.

5.2. *Physical Origin of the Spectral Lag for Individual Pulses*

In this section, we try to clarify the origin of the spectral lag of our HETE-2 GRBs, apart from the lag–luminosity relation described in the preceding sections. First, we need to check whether only the simple curvature effect, which should be in any case included, can explain the energy dependence of the lag or not. Here, we consider the curvature-effect model described by Lu et al. (2006). They calculated the light curves from an isotropically expanding sphere with a constant bulk Lorentz factor and the Band function for a rest-frame radiation spectrum. A Gaussian pulse was assumed for the light curve in the source rest frame. While the generic formula for the spectral lag is complicated, they demonstrated that the spectral lag has an energy dependence with lag $\propto E$ below a saturated energy, $E_{\rm s} = 1.67\,E_{\rm peak}$, for the typical parameter sets of the low-energy index, $\alpha_{\rm B} = -1$, the high-energy index, $\beta_{\rm B} = -2.25$, and the shell radius, $r_0 = 3 \times 10^{15}$ cm. Considering the beaming effect, photons of energy at $E > E_{\rm s}$ would mainly come from the area of the surface around the line of sight, i.e., $\theta \lesssim \Gamma^{-1}$ (where θ is the angle to the line of sight). When $E > E_{\rm s}$, the contribution to the corresponding light curve largely comes from the high-energy portion of the rest-frame spectrum, which causes the peak time of the light curve to change less, and the lag would saturate. On the other hand, for $E < E_{\rm s}$, "off-axis" ($\theta > \Gamma^{-1}$) photons may contribute to the light curve so that the lag increases with the increasing energy difference in the two energy bands.

We choose the peak time at the lowest energy ($\sim$1 keV) arbitrarily to match the observational value of $T_{\rm peak}$. Lu et al. (2006) showed that the lag does not depend strongly on the radius, r_0. Thus, based on their results, we write approximately

$$\tau_{\rm lag} = \begin{cases} a\,E, & \text{if } E \le E_{\rm s} \\ a\,E_{\rm s}, & \text{if } E_{\rm s} < E, \end{cases} \tag{15}$$

$$\text{where } a = 10^{-2.4}\left(\frac{\Gamma}{100}\right)^{-2.8} [\text{s keV}^{-1}]. \tag{16}$$

Then, $T_{\rm peak}$ is written as

$$T_{\rm peak} = t_0 - \tau_{\rm lag} = \begin{cases} t_0 - a\,E, & \text{if } E \le E_{\rm s} \\ t_0 - a\,E_{\rm s}, & \text{if } E_{\rm s} < E, \end{cases} \tag{17}$$

where t_0 is the peak time at the lowest energy. Using equation (17), we tried to reproduce the spectral lag for the examined pulses with the curvature effect by adjusting the bulk Lorentz factor, Γ, in figures 6 and 7. Here, the energy and $T_{\rm peak}$ were translated into the burst rest frame ones with known redshifts, and for GRB 030725 and GRB 060121 without known redshifts, assuming that their redshifts are 1. Although our fits were based on an empirical formula with a particular parameter set ($\alpha_{\rm B} = -1$, $\beta_{\rm B} = -2.25$), the data points do not largely contradict the tendency predicted by the curvature effect at a particular bulk Lorentz factor Γ, as shown in figure 6. However, for some pulses, such as the 2nd pulse of GRB 021211, the 2nd pulse of GRB 040924, the 2nd pulse of GRB 050408, and GRB 030725, the model we adopted could not reproduce the spectral lag well, as shown in figure 7. Even for such pulses, changing the parameters that we have fixed here may soften the contradictions. Alternatively, the off-axis model or the temporal evolution of the internal shock propagation may play an important role in the spectral lag, or a pulse-overlap effect may be included.

To examine whether the pulse duration and spectral lag are explained synthetically by the curvature effect, we summarize the results of the estimated Γ, $\alpha_{\rm w}$, and other properties in table 3. An empirical formula based on Lu et al. (2006) was derived from the assumption for the intrinsic pulse duration, $\Delta t_{\rm int} = 10^5$ s, in the source frame. Although there is no reason to adopt this value, the resultant timescales estimated from the obtained Γ are on the same order of magnitude as 10^5 s. Even for the GRBs whose the spectral lag can be explained by the curvature effect, it is hard to confirm consistency between the prediction of the energy dependence of the pulse duration by the curvature effect ($\alpha_{\rm w} = -0.2 \sim -0.1$) and the experimental values, because of the large uncertainties in $\alpha_{\rm w}$. However, we may say that the model based on the curvature effect does not contradict both the spectral lag and the duration at a particular bulk Lorentz factor, Γ. Thus, the spectral lag can be a tool for estimating the bulk Lorentz factors.

Since in this analysis only a finite energy range (2–400 keV) is available, there are only a small number of points for the energy range, where the lag is saturated above $E_{\rm s}$. For many GRBs, we could only plot one point above $E_{\rm s}$, which rules out the possibility that a significant lag takes place above $E_{\rm s}$ (no saturated energy). Even in a study by Liang et al. (2006), although the peak energy, $E_{\rm peak}$, is $\sim$54 keV, they could also plot only one point for $T_{\rm peak}$ above $E_{\rm peak}$ due to the poor

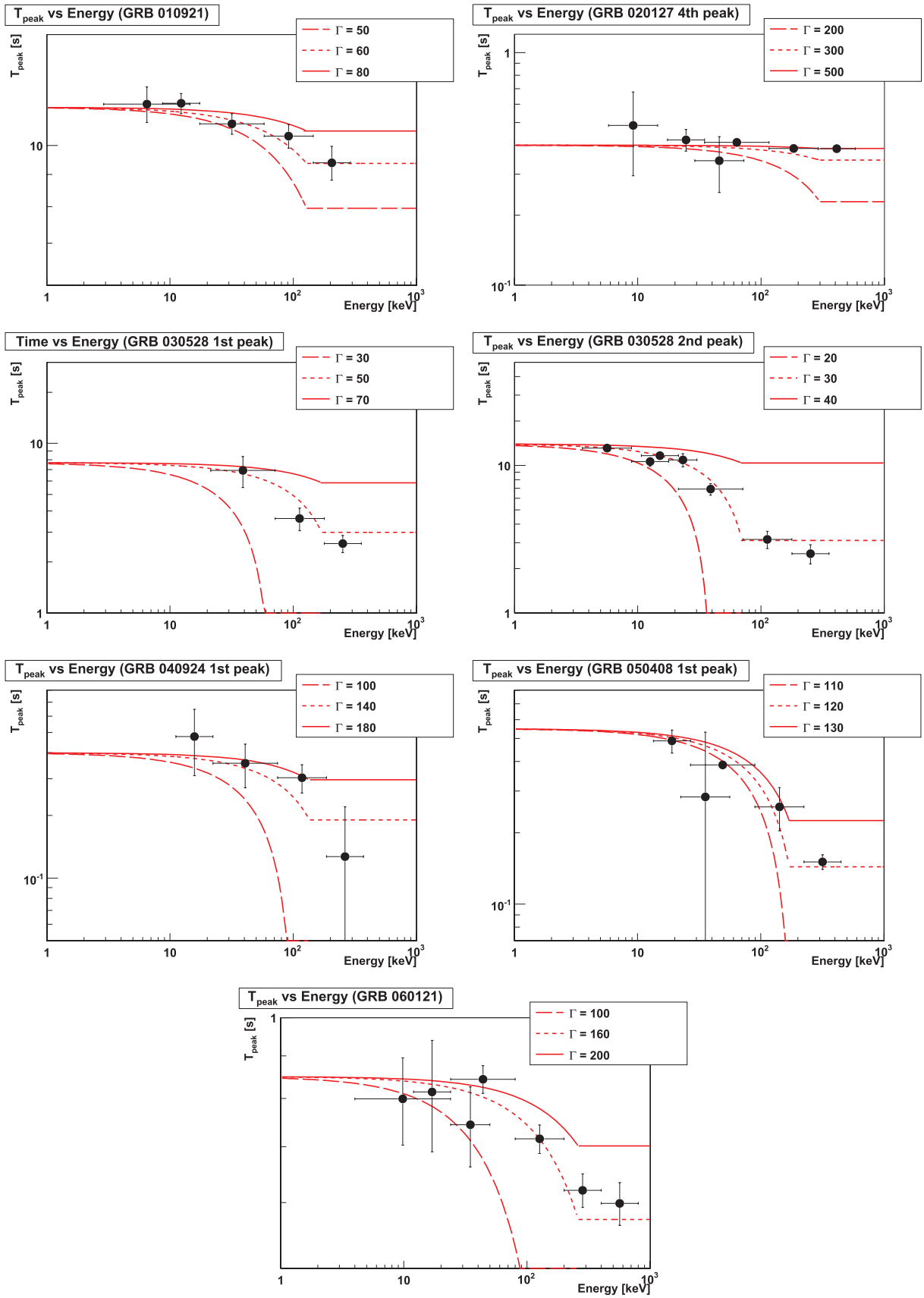

Fig. 6. Energy vs. $T_{\rm peak}$ plots in the burst rest frame with the theoretical model lines, being in agreement with the curvature case. Each line represents the curvature-effect line at the corresponding bulk Lorentz factor, Γ.

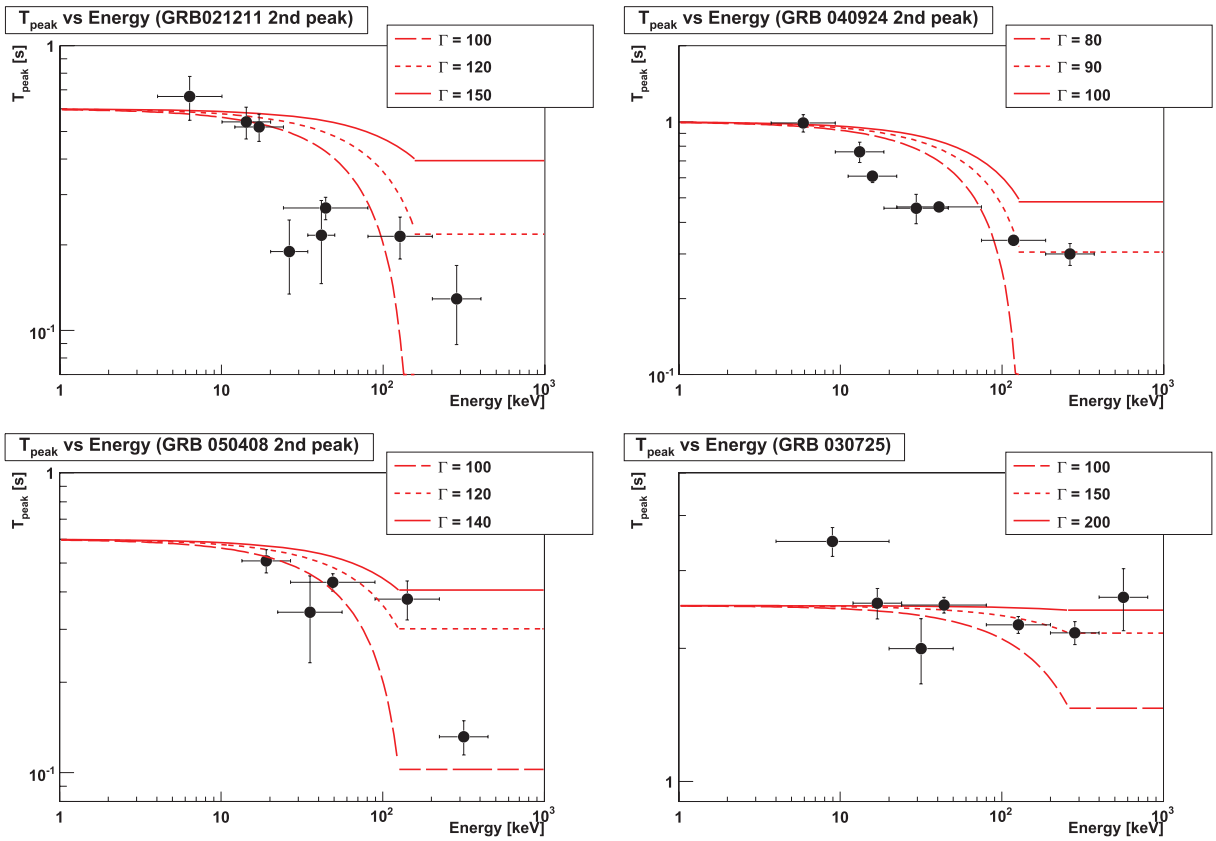

Fig. 7. Energy vs. $T_{\rm peak}$ plots in the burst rest frame with the theoretical model lines, being not in agreement with the curvature case. Each line represents the curvature-effect line at the corresponding bulk Lorentz factor, Γ.

Table 3. Summary of the obtained bulk Lorentz factor, the power-law index of the duration, the observed duration, and the expected intrinsic pulse width.*

GRB	Γ	$\alpha_{\rm w}$	$w_{\rm obs}$ [s]	$\Delta t_{\rm int}^{\rm exp}$ [s]
010921	60	-0.11 ± 0.18	21.4 ± 2.9	0.77×10^5
020127 (4th pulse)	500	-0.67 ± 0.34	0.70 ± 0.01	1.75×10^5
030528 (1st pulse)	50	-0.63 ± 0.61	26.1 ± 14.7	0.65×10^5
030528 (2nd pulse)	30	-0.42 ± 0.15	58.8 ± 6.8	0.53×10^5
040924 (1st pulse)	140	-0.18 ± 0.47	1.8 ± 0.5	0.35×10^5
050408 (1st pulse)	120	-0.20 ± 0.30	2.8 ± 0.2	0.40×10^5
060121	160	-0.42 ± 0.17	1.8 ± 0.2	0.46×10^5
021211 (2nd pulse)	—	-0.58 ± 0.14	2.4 ± 0.1	—
030725	—	-0.18 ± 0.07	19.7 ± 0.5	—
040924 (2nd pulse)	—	-0.51 ± 0.19	1.4 ± 0.1	—
050408 (2nd pulse)	—	-0.22 ± 0.36	2.0 ± 0.2	—

* Note that the bulk Lorentz factor, Γ, is estimated by the lag analysis in figure 6, and $w_{\rm obs}$ is the observed duration in the burst rest frame and $\Delta t_{\rm int}^{\rm exp}$ is the expected intrinsic pulse width from the obtained bulk Lorentz factor, Γ.

effective area for the higher energy ranges. To clarify the origin of the spectral lag further, we need to detect GRB photons in the higher energy ranges above $E_{\rm peak}$ to describe the light curve and determine $T_{\rm peak}$ with confidence.

6. Toward a Unified Theory

Our results suggest that there are correlations between the spectral lag and other observational properties for each GRB pulse. The correlations that we found, and some additional pulse correlations, such as the spectral hardness, pulse

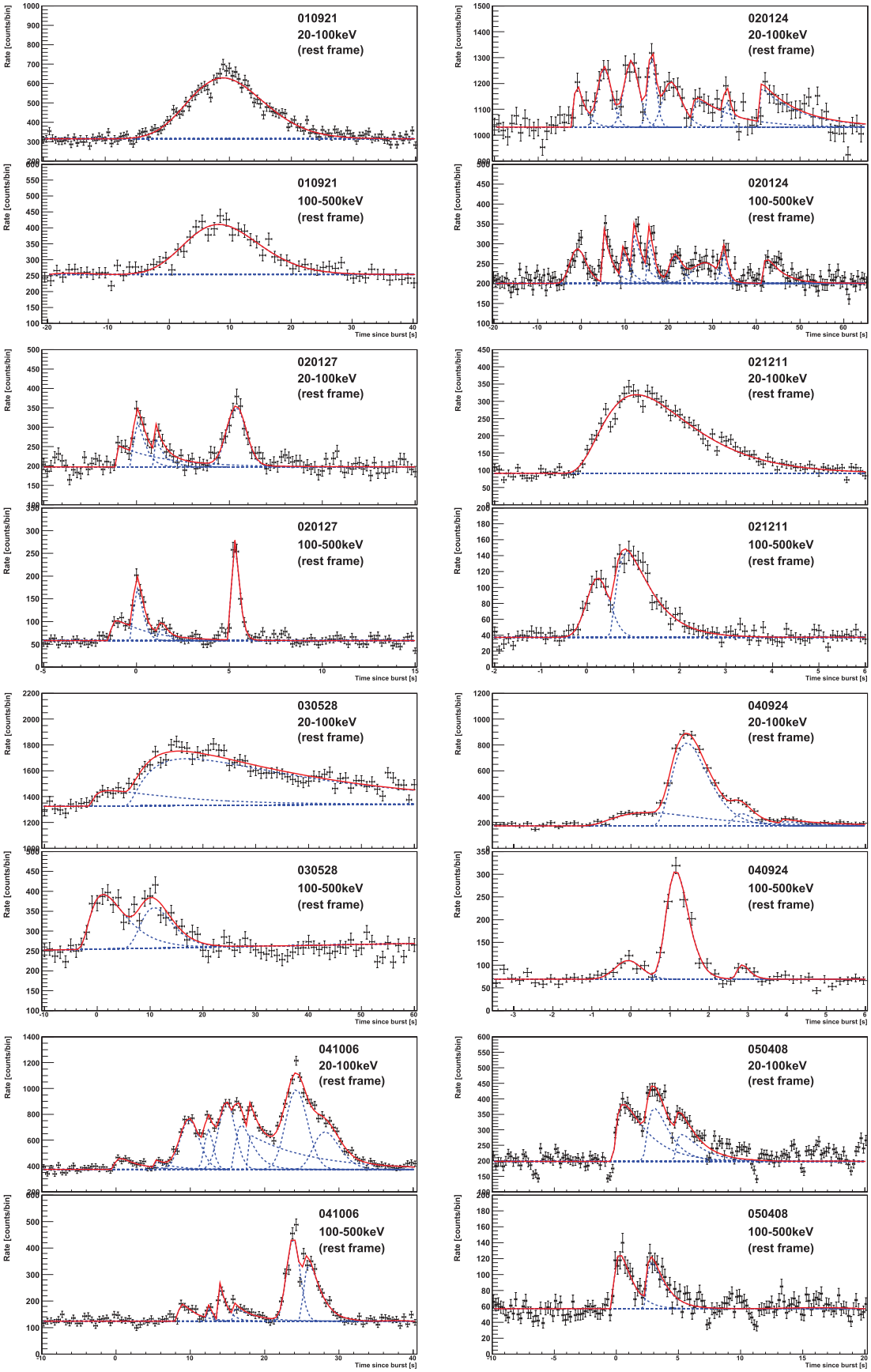

Fig. 8. Result of the fitted pulses in the burst rest frame (20–100 keV and 100–500 keV).

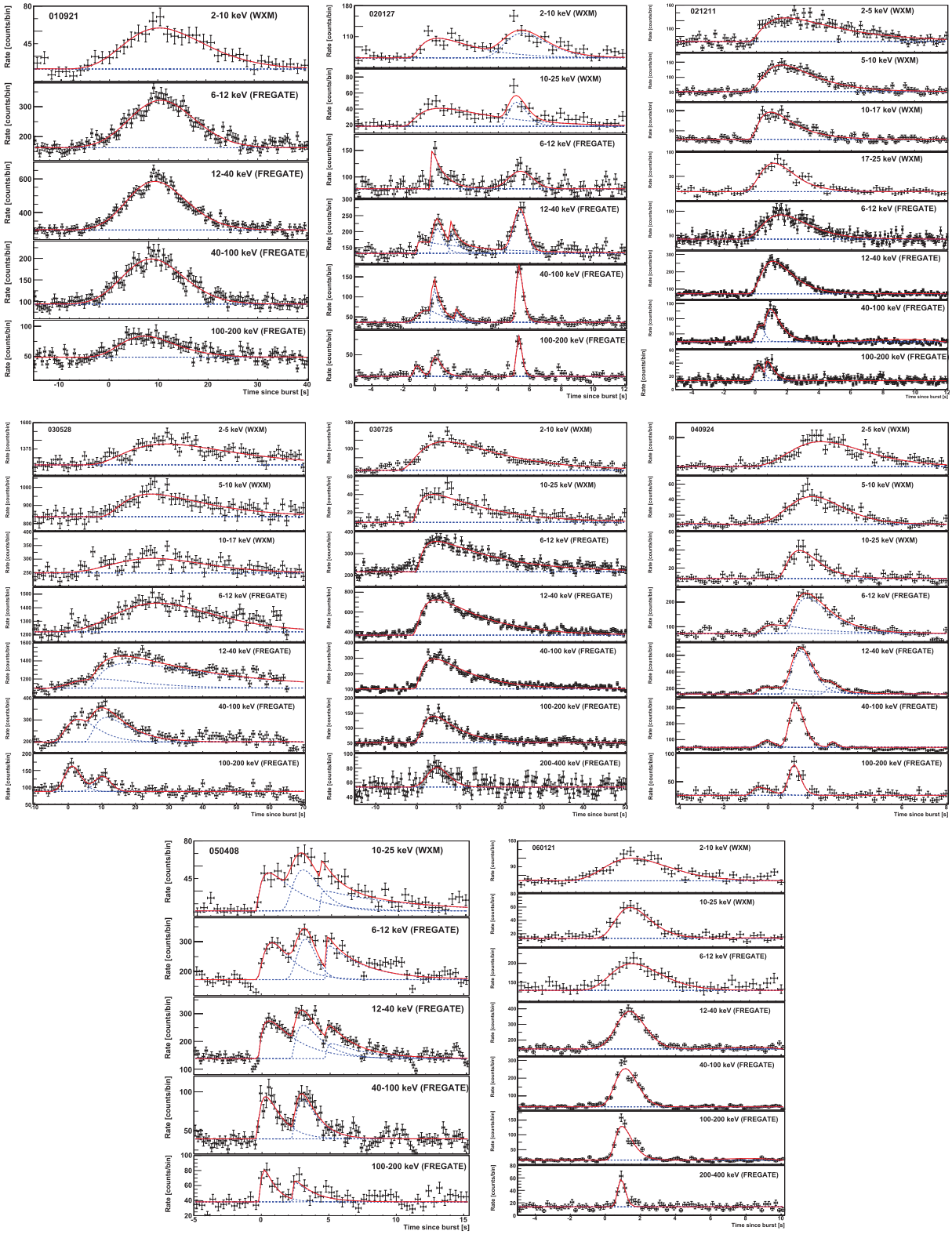

Fig. 9. Result of fitted pulses in multiple energy bands.

asymmetry, etc. reported by Hakkila and Cumbee (2009), are important hints as how to specify or constrain models of GRB prompt emission.

On the other hand, because of the large dispersions, the spectral lag relations are not so useful as tools for measuring cosmological distances so far, compared with the Yonetoku relation. We should note that there may still be systematic uncertainties in the obtained lags, which may change the correlations, as discussed in sub-subsection 4.3.2. While the obtained relations of the lag–luminosity, lag–$E_{\rm peak}$, and lag–duration can be consistent with a specific model, namely the off-axis model suggested by Ioka and Nakamura (2001), the energy dependences of the spectral lag seem to be consistent with the simple curvature effects for some GRB pulses. Because the assumptions inferred in Ioka and Nakamura (2001) and Lu et al. (2006) are different, we have discussed the correlations and energy-dependences in the spectral lag with two independent models. Although such methods do not give us a consistent picture for the spectral lag so far, the discussion presented in this paper may help to determine which models are more appropriate.

For a unified theory to explain the spectral lag and other temporal spectral characteristics, the effect of the curvature, viewing with an offset angle to the jet, time-evolution of shock propagation, and other effects must be taken into account synthetically, and theoretical investigations need to be made. To have further quantitative discussions, we need a sample that includes many GRBs having a good S/N ratio detected in a wide band (keV–GeV) with observationally known redshifts.

We appreciate the referee, Prof. Jon Hakkila, for his fruitful comments, which have improved our paper. M. Arimoto acknowledges financial support from the Global Center of Excellence Program by the Ministry of Education, Culture, Sports, Science and Technology (MEXT) of Japan through the Nanoscience and Quantum Physics Project of the Tokyo Institute of Technology. This work has been supported by a Grant-in-Aid for Young Scientists (B) 20740102 from the MEXT. G. Pizzichini acknowledges financial support from the Italian Space Agency (ASI) via contract I/088/06/0.

References

Band, D., et al. 1993, ApJ, 413, 281
Berger, E., Fox, D. B., Kulkarni, S. R., Frail, D. A., & Djorgovski, S. G. 2007, ApJ, 660, 504
Berger, E., Gladders, M., & Oemler, G. 2005, GCN Circ., 3201
Bošnjak, Ž., Daigne, F., & Dubus, G. 2009, A&A, 498, 677
Daigne, F., & Mochkovitch, R. 1998, MNRAS, 296, 275
Daigne, F., & Mochkovitch, R. 2003, MNRAS, 342, 587
de Ugarte Postigo, A., et al. 2006, ApJ, 648, L83
Djorgovski, S. G., et al. 2001, GCN Circ., 1108
Hakkila, J., & Cumbee, R. S. 2009, in AIP Conf. Proc., 1133, Gamma Ray Burst: Sixth Huntsville Symp., ed. C. Meegan et al. (New York: AIP), 379
Hakkila, J., Giblin, T. W., Norris, J. P., Fragile, P. C., & Bonnell, J. T. 2008, ApJ, 677, L81
Hakkila, J., & Nemiroff, R. J. 2009, ApJ, 705, 372
Hjorth, J., et al. 2003, ApJ, 597, 699
Ioka, K., & Nakamura, T. 2001, ApJ, 554, L163
Liang, E.-W., Zhang, B.-B., Stamatikos, M., Zhang, B., Norris, J., Gehrels, N., Zhang, J., & Dai, Z. G. 2006, ApJ, 653, L81
Lu, R.-J., Peng, Z.-Y., & Dong, W. 2007, ApJ, 663, 1110
Lu, R.-J., Qin, Y.-P., Zhang, Z.-B., & Yi, T.-F. 2006, MNRAS, 367, 275
Norris, J. P., Bonnell, J. T., Kazanas, D., Scargle, J. D., Hakkila, J., & Giblin, T. W. 2005, ApJ, 627, 324
Norris, J. P., Marani, G. F., & Bonnell, J. T. 2000, ApJ, 534, 248
Peng, Z. Y., Ma, L., Zhao, X. H., Yin, Y., Fang, L. M., & Bao, Y. Y. 2009, ApJ, 698, 417
Pugliese, G., et al. 2005, A&A, 439, 527
Qin, Y.-P. 2002, A&A, 396, 705
Qin, Y.-P., & Lu, R.-J. 2005, MNRAS, 362, 1085
Qin, Y.-P., Zhang, Z.-B., Zhang, F.-W., & Cui, X.-H. 2004, ApJ, 617, 439
Rau, A., Salvato, M., & Greiner, J. 2005, A&A, 444, 425
Shen, R.-F., Song, L.-M., & Li, Z. 2005, MNRAS, 362, 59
Stanek, K. Z., et al. 2005, ApJ, 626, L5
Vreeswijk, P., Fruchter, A., Hjorth, J., & Kouveliotou, C. 2003, GCN Circ., 1785
Wiersema, K., Starling, R. L. C., Rol, E., Vreeswijk, P., & Wijers, R. A. M. J. 2004, GCN Circ., 2800
Yonetoku, D., Murakami, T., Nakamura, T., Yamazaki, R., Inoue, A. K., & Ioka, K. 2004, ApJ, 609, 935
Zhang, F.-W., Qin, Y.-P., & Zhang, B.-B. 2007, PASJ, 59, 857